The exchange bias effect in phase separated $Nd_{1-x}Sr_xCoO_3$ at the spontaneous ferromagnetic/ferrimagnetic interface

2009 J. Phys.: Condens. Matter 21 236004

(http://iopscience.iop.org/0953-8984/21/23/236004)

J. Phys.: Condens. Matter **21** (2009) 236004 (8pp) doi:10.1088/0953-8984/21/23/236004

The exchange bias effect in phase separated $Nd_{1-x}Sr_xCoO_3$ at the spontaneous ferromagnetic/ferrimagnetic interface

M Patra, M Thakur, S Majumdar and S Giri

Department of Solid State Physics, Indian Association for the Cultivation of Science, Jadavpur, Kolkata 700 032, India
and
Center for Advanced Materials, Indian Association for the Cultivation of Science, Jadavpur, Kolkata 700 032, India

E-mail: sspsg2@iacs.res.in (S Giri)

Received 20 February 2009, in final form 1 April 2009
Published 7 May 2009
Online at stacks.iop.org/JPhysCM/21/236004

Abstract

We report new results for the exchange bias effect in $Nd_{1-x}Sr_xCoO_3$ for $x = 0.20$ and 0.40, where the exchange bias phenomenon is involved with the ferrimagnetic (FI) state in a spontaneously phase separated system. The zero-field-cooled magnetization exhibits FI (T_{FI}) and ferromagnetic (FM; T_C) transitions at ~23 and ~70 K, respectively, for $x = 0.20$. Negative horizontal and positive vertical shifts of the magnetic hysteresis loops are observed when the system is cooled through T_{FI} in a positive static magnetic field. A training effect is observed for $x = 0.20$, which could be interpreted satisfactorily by the spin configurational relaxation model. The unidirectional shifts of the hysteresis loops as a function of temperature exhibit an absence of exchange bias above T_{FI} for $x = 0.20$. Analysis of the cooling field dependence of the exchange bias field and magnetization indicates that the FM clusters consist of a single magnetic domain with an average size of around ~20 and ~40 Å for $x = 0.20$ and 0.40, respectively. The sizes of the FM clusters are close to the percolation threshold for $x = 0.20$; these grow and coalesce to form the bigger size for $x = 0.40$ resulting in a weak exchange bias effect.

(Some figures in this article are in colour only in the electronic version)

1. Introduction

Exchange bias (EB) coupling in a heterogeneous system composed of soft and hard magnetic substances gives rise to unidirectional anisotropy at the interface when the sample is cooled down to a low temperature through the critical temperature of the hard magnetic component in an external magnetic field [1]. It manifests itself by a shift of the hysteresis loop and enhancement of coercivity, which attract considerable attention because of potential applications in magnetic memories, spin-electronics, etc. Numerous reports are found on the EB phenomenon at artificial interfaces; these have mainly been focused on the development of advanced materials for the application and understanding of the complex EB phenomenon [2–5]. However, the signature of the EB effect is rarely observed in compounds with a unique crystal structure and having a spontaneous interface. The first example of the EB effect without an artificial interface was reported in 1961 [6] for Cu(Mn) and Ag(Mn) alloys, which have been recognized as typical spin-glass (SG) and cluster-glass (CG) systems depending on the dilution limit. Recently, the signature of the EB effect has been reported at spontaneous interfaces for few mixed-valent manganites and cobaltites with a perovskite structure [7–11]. The first report was observed in a charge ordered (CO) compound, $Pr_{1/3}Ca_{2/3}MnO_3$, where ferromagnetic (FM) droplets were spontaneously embedded in an antiferromagnetic (AFM) background creating a FM/AFM interface [7]. The EB phenomenon was reported for another

CO manganite $Y_{0.2}Ca_{0.8}MnO_3$, where a strong cooling field dependence of EB was observed due to a considerable change in the phase fraction between FM/AFM layers [8]. Recently, we observed the signature of the EB phenomenon in the cluster-glass (CG) compounds $LaMn_{0.7}Fe_{0.3}O_3$ and $La_{0.87}Mn_{0.7}Fe_{0.3}O_3$ [9, 12], where short range FM clusters were embedded in a SG-like matrix creating a spontaneous FM/SG interface [9, 13–15]. The average size of the FM clusters was found to decrease systematically with decreasing particle size, which had a strong influence on the EB phenomenon. The EB field was found to increase significantly with decreasing particle size, which was attributed to the increase of interface area by decreasing particle size [16, 17].

The mixed-valent cobaltites with perovskite structure experience a delicate interplay between charge, spin state, transport, magnetic and structural degrees of freedom, exhibiting a complex phase separation scenario. An interesting phase diagram has been proposed for the hole doped compound $Nd_{1-x}Sr_xCoO_3$ depending on the degree of hole doping [18]. For the low doping range ($0 < x < 0.18$) the SG or CG state has been proposed with resistivity showing a semiconducting temperature dependence. With further increase in hole doping the short range FM clusters begin to coalesce above a percolation threshold ($x > 0.18$) to attain magnetic long range ordering and start to show metallic conductivity in the ordered state. Metallic conductivity in both the paramagnetic and ordered states is observed for $x \geqslant 0.28$. The coexistence of ferrimagnetic (FI) and FM ordering is reported for $0.20 \leqslant x \leqslant 0.60$. Neutron powder diffraction studies on $Nd_{0.67}Sr_{0.33}CoO_3$ confirm that the FM (T_C) and FI (T_{FI}) ordering temperatures are ∼200 and ∼40 K, respectively, where ferrimagnetism was interpreted in terms of an induced antiparallel ordering of the Nd spins in close proximity to the Co sublattice [19]. Several reports of electrical, magnetic and thermodynamic studies of $Nd_{1-x}Sr_xCoO_3$ also suggest the coexistence of FI and FM ordering for $x = 0.33$ and 0.50 [20–22]. ^{59}Co NMR studies on $Nd_{1-x}Sr_xCoO_3$ ($0 \leqslant x \leqslant 0.50$) confirm different spin states of Co^{3+} and Co^{4+} ions [23]. The parent compound $NdCoO_3$ shows the low spin (LS) state of the Co^{3+} ion in the paramagnetic state. As a result of hole doping ($0.10 \leqslant x \leqslant 0.20$) an intermediate spin (IS) state of Co^{3+} and Co^{4+} appears in addition to the LS state of Co^{3+}, and the LS state of Co^{3+} no longer exists with further increase in hole doping ($0.30 \leqslant x \leqslant 0.50$). The reported results indicate that the magnetic and electronic phase separation scenario of $Nd_{1-x}Sr_xCoO_3$ is very similar to that in $La_{1-x}Sr_xCoO_3$ except for the fact that the Nd ion carries moment, unlike the La ion [24].

Recently, the signature of the EB phenomenon ascribed to the intrinsic inhomogeneous phase separation was reported in the CG compounds $La_{1-x}Sr_xCoO_3$ ($0.12 \leqslant x \leqslant 0.30$), where EB was suggested to be due to the CG state consisting of FM and SG phases [10, 11]. In order to observe the EB phenomenon the system must involve reversible and rigid phases, where magnetization of the first one can be reversed while that of the second one cannot be. EB is observed in $La_{1-x}Sr_xCoO_3$ at the reversible FM and rigid SG interface. The phase separated compounds $Nd_{1-x}Sr_xCoO_3$ also exhibit the necessary ingredients for the EB effect, where spontaneous phase separation between FM and FI states exists giving rise to a FM/FI interface for $x \geqslant 0.18$. Here, the EB phenomenon is investigated in $Nd_{1-x}Sr_xCoO_3$ with $x = 0.20$ and 0.40, where the first one is close to the percolation threshold with semiconducting behavior and the second one exhibits metallic conductivity, where percolation has already set in. We observe the EB effect for both the samples, where the effect is strong for $x = 0.20$ and weak for $x = 0.40$. In order to explain different EB effects for both compounds a nanoscale phase separation scenario has been proposed in $Nd_{1-x}Sr_xCoO_3$ for $x \geqslant 0.20$. So far the EB phenomenon has been reported for manganites and cobaltites with perovskite structures at spontaneous FM/AFM and FM/SG interfaces. Here, we present a new example of the EB effect in the spontaneously phase separated compounds $Nd_{1-x}Sr_xCoO_3$ for $x \geqslant 0.20$, where the EB effect is involved with the FI states.

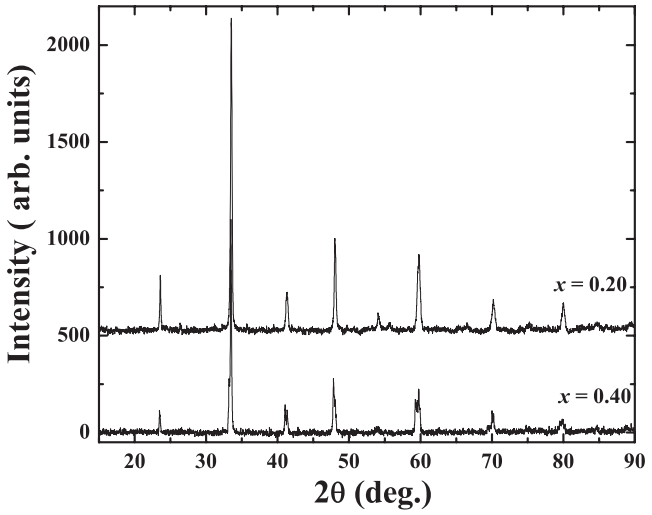

Figure 1. X-ray powder diffraction patterns at room temperature for $Nd_{1-x}Sr_xCoO_3$ with $x = 0.20$ and 0.40. The base line of the plot for $x = 0.20$ is shifted vertically upwards for clarity.

2. Experimental details

The polycrystalline compounds $Nd_{1-x}Sr_xCoO_3$ with $x = 0.20$ and 0.40 were prepared by the chemical citrate route, which was described in our earlier report [13]. Stoichiometric proportions of Nd_2O_3, $SrCO_3$ and Co powders were dissolved in an aqueous solution of nitric acid and mixed thoroughly. Citric acid was then added to the solution to achieve a homogeneous mixture of metal citrates. The metal citrates were dried and decomposed at 873 K for 6 h. Finally, the powdered samples were pressed into pellets and heated at 1273 K for 6 h followed by slow cooling at a rate of 0.7 K min^{-1}. The single orthorhombic ($Pbnm$) structure at room temperature is confirmed for both the compounds, where x-ray powder diffraction (Seifert XRD 3000P) was recorded using Cu Kα radiation. We did not observe any impurity phase in the x-ray diffraction patterns, which are shown in figure 1. The values of the lattice parameters are 5.35 (a), 5.36 (b) and 7.56 (c) Å for $x = 0.20$, while for $x = 0.40$ the parameters are 5.40 (a), 5.35 (b)

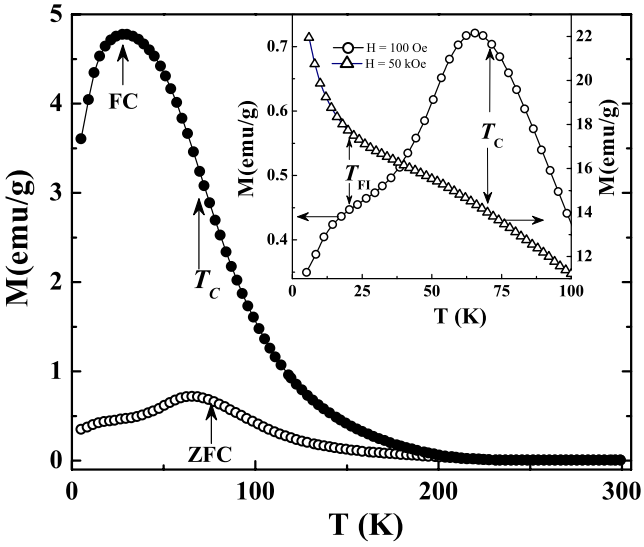

Figure 2. Temperature dependence of magnetization measured at 100 Oe under zero-field-cooled (ZFC) and field-cooled (FC) conditions for $x = 0.20$. The inset shows the ZFC magnetization highlighting ferrimagnetic (T_{FI}) and ferromagnetic (T_C) transitions for the measurements at 100 Oe and 50 kOe.

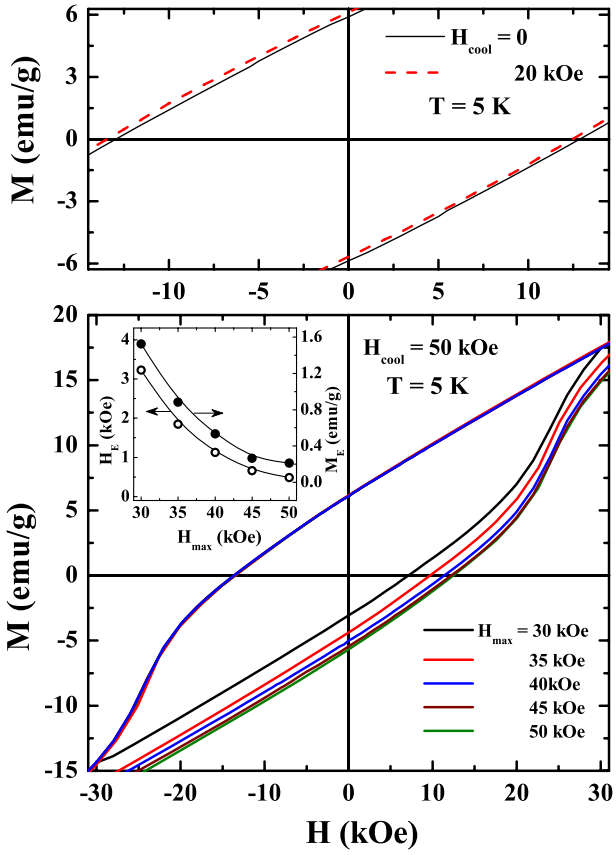

Figure 3. Top panel: central part of the hysteresis loops at 5 K measured after cooling the sample in zero field and field at 20 kOe, where loops measured after field cooling are indicated by the broken curve. Bottom panel: central part of the minor loops at 5 K for measurements between ±30, ±35, ±40, ±45 and ±50 kOe after cooling the sample with 50 kOe. The inset exhibits the variation of the exchange bias field (H_E) and magnetization (M_E) with H_{max} for $x = 0.20$.

and 7.61 (c) Å. The lattice parameters are consistent with an earlier report [23]. The average size of the particles is found around ∼150.0 nm for both the compounds, and was confirmed by a transmission electron microscope (TEM; model JEOL JEM-2010). The dc magnetization was measured using a commercial superconducting quantum interference device (SQUID) magnetometer (MPMS, XL). In the case of zero-field-cooled (ZFC) magnetization the sample was cooled down to the lowest temperature in zero field and the magnetization was measured in the warming cycle by applying an external magnetic field. For field-cooled (FC) magnetization the sample was cooled down to a low temperature in a magnetic field and the measurement was performed in the warming cycle like ZFC magnetization.

3. Experimental results

The temperature dependence of ZFC and FC magnetization measured at 100 Oe is shown in figure 2 for $Nd_{0.80}Sr_{0.20}CoO_3$. The inset of the figure exhibits ZFC magnetization highlighting the FI (T_{FI}) and FM (T_C) transitions at ∼23 and ∼70 K, respectively, where T_{FI} is indicated by a shoulder around ∼23 K for the low-field measurement at 100 Oe. A sharp increase in the ZFC magnetization is observed below T_{FI} when the measurement was performed at a high field with 50 kOe. T_C is defined around ∼70 K, where a sharp increase in FC magnetization is observed for the measurement at 100 Oe. The values of T_{FI} and T_C in the present observation are reproduced exactly compared to the values reported by Stauffer *et al* [18].

We observe the horizontal and vertical shifts of the magnetic hysteresis loop when the sample was cooled under the FC mode. A negative shift in the field axis and a positive shift in the magnetization axis are observed at 5 K for a positive cooling field, which is shown in the top panel of figure 3. We define the exchange bias field, $-H_E = (H_{left} + H_{right})/2 \approx -500$ Oe, for the measurement of magnetic hysteresis in between ±50 kOe. Here, H_{right} and H_{left} are the positive and negative values of field at magnetization $M = 0$, respectively. The value of M_E/M_S is $\sim 0.53 \times 10^{-2}$, where M_E and M_S are the exchange bias magnetization and saturation of magnetization. The values of the asymmetry parameters involved with the FM and FI states are comparable to those involved with the FM and SG states in cobaltite $La_{1-x}Sr_xCoO_3$, where the maximum effect of EB was reported for hole doped cobaltites [10]. The value of H_E was 500 Oe when hysteresis was measured in between ±50 kOe for $La_{0.88}Sr_{0.12}CoO_3$ [11]. The reported values of the shifts for the phase separated cobaltites are compared in table 1 with the present observations for $x = 0.20$ and 0.40 for different H_{max}, where H_{max} is the maximum field used for the measurement of hysteresis loops. In order to confirm the exchange bias effect the magnetic hysteresis loops were measured at 5 K with different H_{max} in between ±30, ±35, ±40, ±45 and ±50 kOe after cooling the sample with $H_{cool} = 50$ kOe for $x = 0.20$. The central parts of the hysteresis loops are shown in the bottom panel of figure 3. We note that the hysteresis

Table 1. The maximum values of exchange bias field (H_E) and relative vertical shift (M_E/M_S) at different types of interfaces (ferromagnetic (FM)/spin-glass (SG) and FM/ferrimagnetic (FI)) for phase separated cobaltites measured between different $\pm H_{max}$.

System	H_{max} (kOe)	H_E (kOe)	M_E/M_S (10^{-2})	Interface
$La_{0.88}Sr_{0.12}CoO_3$ [11]	50	0.50	0	FM/SG
$Nd_{0.80}Sr_{0.20}CoO_3$[a]	50	0.50	0.53	FM/FI
$Nd_{0.60}Sr_{0.40}CoO_3$[a]	50	0.08	0.55	FM/FI

[a] Current investigation.

loops measured in between ±45 and ±50 kOe almost merge together. The values of H_E and M_E as a function of H_{max} are shown in the inset of the figure. The values of H_E and M_E decrease with increasing H_{max}, showing an indication of stabilization for $H_{max} \geqslant 45$ kOe, where the values of H_E and M_E at $H_{cool} = 50$ kOe are significantly large (see table 1). Thus the EB effect obtained for measurements of the hysteresis loop between ±50 kOe is not a minor loops effect [25], rather it supports the EB effect. The H_{max} dependence of H_E and M_E has also been investigated by Salazar-Alvarez *et al* for MnO/Mn_3O_4 core/shell structure, where the plots confirmed the non-zero asymptotic value of the horizontal shift at $H_{max} =$ 70 kOe attributed to the EB effect [26]. In order to confirm this further we investigate the training effect, which is one of the important features of a system exhibiting EB effect.

A training effect is described by the decrease of H_E and M_E when the system is successively field cycled at a particular temperature after field cooling [4, 7, 10]. We investigate the training effect for $x = 0.20$, where the sample was cooled down to 5 from 250 K with $H_{cool} = 20$ kOe and then the hysteresis loops were measured successively in between ±50 kOe up to 16 times. We note that the training effect is evident in the system. The central parts of the 1st, 2nd, 8th and 16th loops are shown in the inset of figure 4. The systematic decrease of H_E and M_E with the consecutive cycling number (λ) is shown in figure 4 by the open symbols. The values of H_E and M_E are decreased up to ∼10% and ∼11%, respectively, for $\lambda = 2$, and are smaller than the values reported for the SG based systems—a ∼19% decrease of H_E ($\lambda = 2$) for $La_{0.82}Sr_{0.18}CoO_3$ [10] and a ∼40% decrease of H_E ($\lambda = 2$) for the Fe/FeO nanogranular system [27]. In the present investigation the small decreases of H_E and M_E further indicate that exchange coupling is involved with the FI based system, not with the typical SG based system. The decrease of H_E (M_E) is fitted satisfactorily with the following empirical relation

$$H_E(\lambda) - H_E^{\infty} \propto \frac{1}{\sqrt{\lambda}}, \qquad (1)$$

where H_E^{∞} is the value for $\lambda \to \infty$. The solid lines in figure 4 exhibit the best fit of H_E and the variation of M_E with λ for $\lambda \geqslant 2$. The values of the fitted parameters are $H_E^{\infty} \approx 377$ Oe and $M_E^{\infty} \approx 0.157$ emu g^{-1}. The above empirical relation does not fit the sharp decrease between first and second loops in accordance with the reported results [4, 7, 10], which might be due to the symmetry effects in the FI matrix [28]. Recently, Binek proposed a recursive formula in the framework of spin

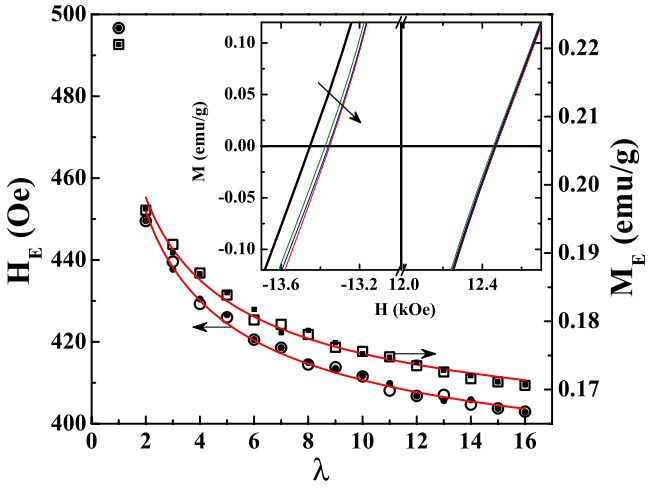

Figure 4. Decrease of the exchange bias field (H_E) and magnetization (M_E) with the consecutive number (λ) of cycles of the hysteresis loop for $x = 0.20$ exhibiting the training effect. The central part of the 1st, 2nd, 8th and 16th loops are shown in the inset, where the arrow indicates the increasing direction of λ.

configurational relaxation to understand the training effect for a FM/AFM heterostructure, which describes the $(\lambda + 1)$th loop shift with respect to the λth one as [29]

$$H_E(\lambda + 1) - H_E(\lambda) = -\gamma[H_E(\lambda) - H_E^{\infty\prime}]^3, \qquad (2)$$

where γ is a sample dependent constant. Using $\gamma = 2.28 \times 10^{-5}$ Oe^{-2} and $H_E^{\infty\prime} = 369.4$ Oe the whole set of data are reproduced for H_E, while the values of γ and $M_E^{\infty\prime}$ are 79.5 (emu g^{-1})$^{-2}$ and 0.153 emu g^{-1}, respectively, for M_E. The calculated values are shown by the filled symbols in figure 4, which match satisfactorily with the experimental data (open symbols). Thus, the spin configurational relaxation model can describe our experimental results satisfactorily, where successive reversal of the FM spins triggers the configurational relaxation of the interfacial FI spins toward equilibrium giving rise to the training effect.

The magnetic hysteresis loops were measured in between ±50 kOe at different temperatures for $Nd_{0.80}Sr_{0.20}CoO_3$ after cooling the sample down to the desired temperatures from 250 K with $H_{cool} = 20$ kOe. The values of coercivity (H_C), H_E and M_E/M_S as a function of temperature are shown in figure 5. H_C decreases slowly and vanishes at the onset of the Curie temperature around ∼70 K. On the other hand, H_E and M_E/M_S decrease sharply with increasing temperature and disappear for $T \geqslant 20$ K, where a shoulder in the ZFC magnetization is observed, indicating the signature of FI ordering. The temperature dependence of the asymmetry parameters are typical for EB systems, namely, charge ordered $Pr_{1/3}Ca_{2/3}MnO_3$ [7], CG $LaMn_{0.7}Fe_{0.3}O_3$ [9] and CG cobaltites $La_{1-x}Sr_xCoO_3$ [10, 11], where the EB effect vanishes above the AFM (T_N) or spin freezing (T_f) transition temperature. In the case of EB systems the rigid AFM or SG spins apply a coupling force on the FM spins at the interface and a layer of pinned or frozen FM spins is created on the outer surface of the FM clusters when the system is cooled

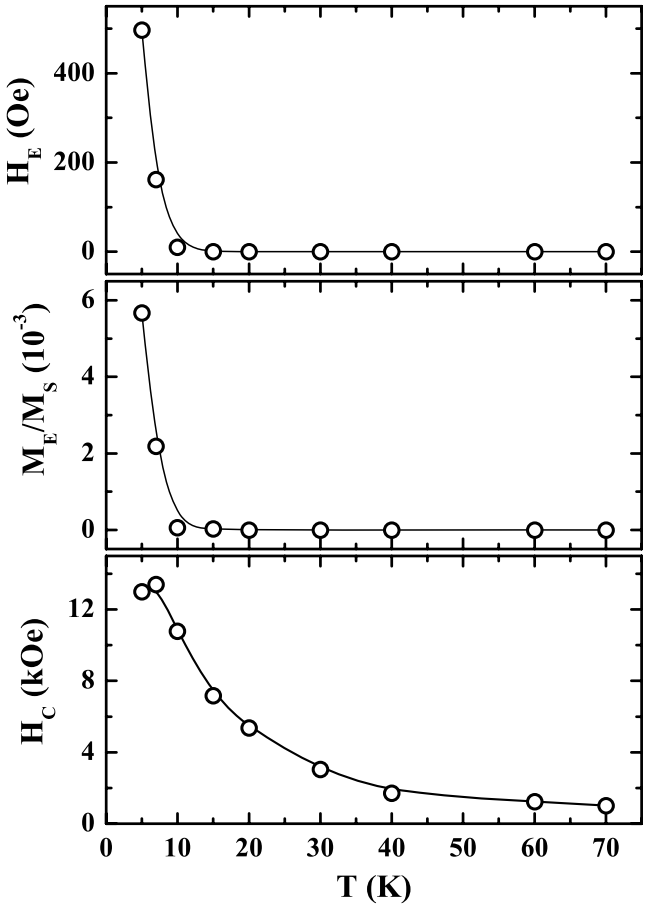

Figure 5. Temperature dependence of (a) exchange bias field (H_E), (b) relative vertical shift (M_E/M_S) and (c) coercivity (H_C) with $H_{cool} = 20$ kOe for $x = 0.20$.

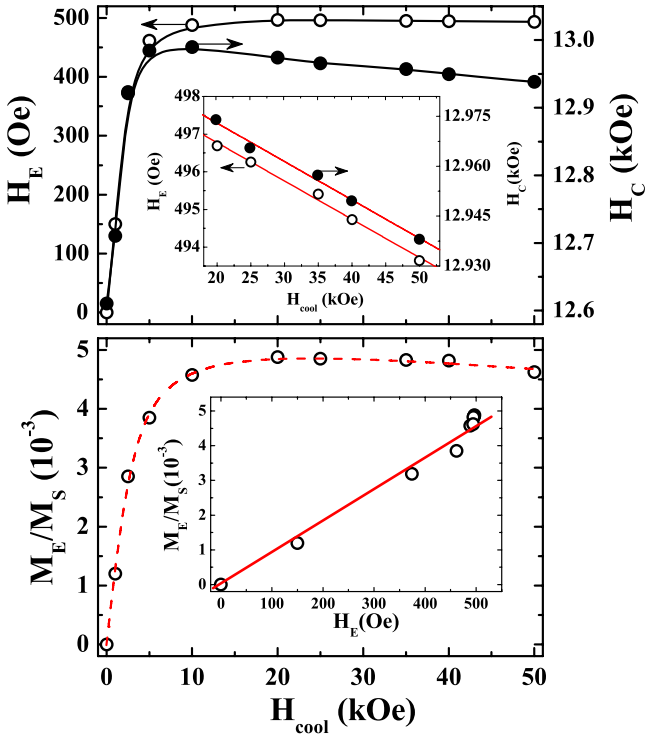

Figure 6. The exchange bias field (H_E) and coercivity (H_C) (top panel) and M_E/M_S (bottom panel) at 5 K for $x = 0.20$ are plotted with cooling field (H_{cool}), where hysteresis loops were measured between ±50 kOe. The H_{cool} dependence of H_E and H_C for $H_{cool} \geqslant 20$ kOe and the plot of M_E/M_S against H_E are shown in the insets of the top and bottom panels, respectively. The broken curve in the bottom panel is the fitted curve using a simplified exchange interaction model. The solid straight lines in the insets show the linear fits.

in FC mode. The pinned or frozen FM spins give rise to the unidirectional shift of the hysteresis loops and reveal the EB effect. For $Nd_{1-x}Sr_xCoO_3$ with $x \geqslant 0.20$ the coexistence of FM and FI phases has been suggested by Stauffer *et al* [18], and is also indicated here by the ZFC magnetization for $x = 0.20$ (inset of figure 2). Therefore, the EB effect below T_{FI} is suggested to be due to the pinning effect. The rigid FI spins operate the pinning force on the reversible FM spins at the FM/FI interface and the pinned FM spins lead to the EB effect. The signature of EB effects involved with the FI phase are reported at the different combinations of artificial interfaces, namely, FM/FI, FI/AFM and FI/FI interfaces, for different bilayer heterostructures [4, 26, 30–33]. Here, we observe the new results of the EB effect at the intrinsic FM/FI interface, where the EB effect is ascribed to spontaneous separation between FM and FI phases.

The cooling field dependence of the EB effect was investigated for $x = 0.20$, where the sample was cooled down to 5 K from 250 K with different cooling fields and the hysteresis loops were measured between ±50 kOe. The H_{cool} dependence of H_E and H_C is shown in the top panel of figure 6. Both of them increase sharply with H_{cool} up to 10 kOe and then shows a slight decreasing trend above 20 kOe. The plots follow a nearly linear dependence above 20 kOe, which is highlighted in the inset of the top panel of figure 6. A very small decrease of H_E around ∼0.6% is noticed at 5 K for the increase of H_{cool} from 20 to 50 kOe. In the high H_{cool} region the feature of H_E is reminiscent to the FM/FI interface analogous to that observed for FM/AFM bilayers [34], AFM-core and FI-shell structures [26] and unlike to that observed for FM/SG systems [9–11, 16, 35]. For the EB systems involved with a SG state the values of H_E are decreased considerably with increasing H_{cool} above a certain value of H_{cool}, where large H_{cool} typically affects the frozen spins in the SG state and frozen FM spins by polarizing it toward the direction of H_{cool}. In fact, H_E decreases up to ∼40% for an increase of H_{cool} from 20 to 50 kOe in $La_{0.88}Sr_{0.12}CoO_3$ [11], ∼47% for an increase of H_{cool} from 6 to 12 kOe in $LaMn_{0.7}Fe_{0.3}O_3$ [9] and ∼25% for an increase of H_{cool} from 2 to 4 kOe in $La_{0.87}Mn_{0.7}Fe_{0.3}O_3$ [12], where the systems are involved with the SG states exhibiting the EB effect. The frozen FM spins and pinned FM spins may have different features with H_{cool}, where the large values of H_{cool} cannot influence the pinned FM spins significantly, which is indicated by the minor change of H_E for the AFM or FI state.

Recently, a simplified exchange interaction model has been proposed by Niebieskikwiat and Salamon considering the FM clusters embedded in an AFM host for a CO compound $Pr_{1/3}Ca_{2/3}MnO_3$ [7]. The FM clusters were assumed to have a single domain structure, which exhibit magnetization

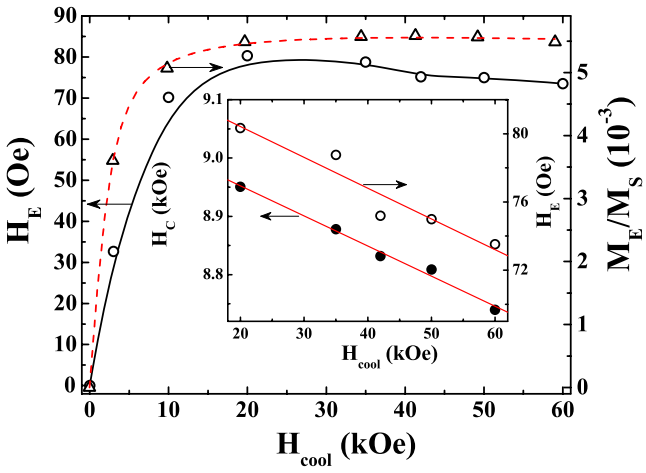

Figure 7. Plots of exchange bias field (H_E) and relative vertical shift (M_E/M_S) against cooling field (H_{cool}) at 5 K for $x = 0.40$. The broken curve is a fit of the H_{cool} dependence of the M_E/M_S plot. The inset shows the plot of H_E and H_C as functions of H_{cool}. Solid straight lines indicate the linear fits.

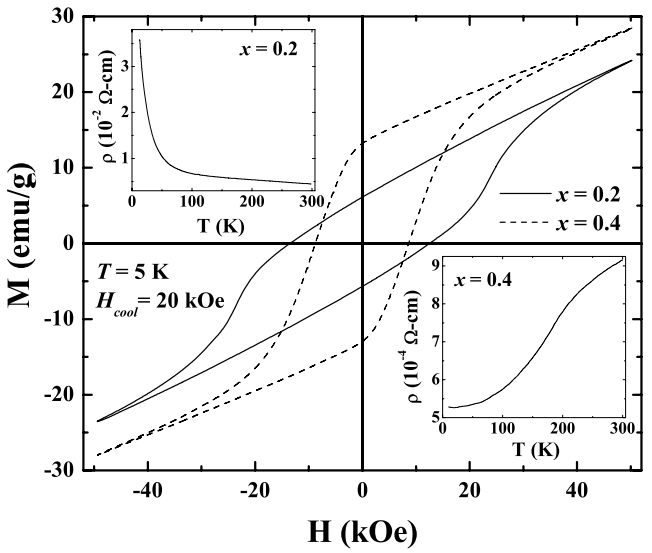

Figure 8. Magnetic hysteresis loop at 5 K after field cooling with 20 kOe for $x = 0.20$ (continuous curve) and $x = 0.40$ (broken curve) for $Nd_{1-x}Sr_xCoO_3$. The upper and lower insets exhibits the temperature dependence of resistivity (ρ) for $x = 0.20$ and 0.40, respectively.

reversal like FM nanoparticles consisting of a single magnetic domain. The model gives the simplified relation between H_E and M_E/M_S as $H_E \propto M_E/M_S$ for $\mu H_E < k_BT$, where M_S and μ are the saturation magnetization and average moment of the FM clusters, respectively. We observe nearly linear behavior between H_E and M_E/M_S in the inset of the bottom panel of figure 6, which has also been verified for $Pr_{1/3}Ca_{2/3}MnO_3$ [7], $CaMnO_{3-\delta}$ [36], $LaMn_{0.7}Fe_{0.3}O_3$ [9, 16] and $La_{0.87}Mn_{0.7}Fe_{0.3}O_3$ [12] exhibiting the EB effect. Here, the value of $\mu H_E/k_BT \approx 0.87$, where the value of μ is obtained from the fit of M_E/M_S against H_{cool} plot, which is described below. Note that the value of $\mu H_E/k_BT$ was ∼0.9 for $Pr_{1/3}Ca_{2/3}MnO_3$ [7]. The linear dependence of the M_E/M_S against H_E plot indicates that FM clusters may have a single domain structure for $Nd_{0.80}Sr_{0.20}CoO_3$. The model further defines the H_{cool} dependence of M_E/M_S as

$$H_E \propto M_E/M_S \propto j_i\left[\frac{j_i\mu_0}{(g\mu_B)^2}L\left(\frac{\mu H_{cool}}{k_BT_f}\right) + H_{cool}\right], \qquad (3)$$

which was verified successfully for spontaneously phase separated $Pr_{1/3}Ca_{2/3}MnO_3$ [7], $LaMn_{0.7}Fe_{0.3}O_3$, [9, 16] and $La_{0.87}Mn_{0.7}Fe_{0.3}O_3$ [12]. The first term in the expression dominates for small H_{cool}, whereas the second term dominates for large H_{cool}, which varies linearly with H_{cool}. In the above relation J_i and μ are adjustable parameters, where J_i is the interface exchange constant. T_f in the above expression was defined as the freezing temperature below which M_E/M_S was found to increase steeply for $Pr_{1/3}Ca_{2/3}MnO_3$. Here, we assume the value of $T_f \sim 15$ K below which M_E/M_S increases sharply. The broken curve in the bottom panel of figure 6 exhibits a satisfactory fit of the experimental data using the above expression. The number density of FM clusters (n) is estimated from the saturation magnetization, $M_S \approx n\mu$, where the value of M_S at 5 K is obtained from the extrapolation of the magnetization at $1/H \rightarrow 0$. The value of n is $\approx 15.5 \times 10^{-5}$ Å^{-3} which further gives the rough estimate of the size of the FM clusters around ∼20 Å. The value of the size of the FM cluster is consistent with those around ∼10 Å for $Pr_{1/3}Ca_{2/3}MnO_3$ [7] and ∼10–30 Å for $LaMn_{0.7}Fe_{0.3}O_3$ depending on the particle size [16].

We also investigate the EB effect for $x = 0.40$, where the maximum values of H_E and M_E/M_S are shown in table 1. The value of M_E/M_S is nearly the same, whereas H_E is much smaller for $x = 0.40$ than that of the value for $x = 0.20$. The H_{cool} dependence of the EB effect was also measured for $x = 0.40$. The plots of H_E and M_E/M_S as a function of H_{cool} at 5 K are shown in figure 7. H_E is found to increase sharply up to ∼20 kOe and shows a decreasing trend with the further increase of H_{cool}, where M_E/M_S follows an almost similar behavior. The linear dependence of M_E/M_S against H_E is observed for $x = 0.40$ analogous to $x = 0.20$, which indicates that the FM clusters of $x = 0.40$ also have a single domain structure. We observe the linear H_{cool} dependence of H_E and H_C above 20 kOe, which is shown in the inset of figure 7. Here, a very small decrease of H_E (∼0.5%) is also observed for $x = 0.40$, like for $x = 0.20$. The model proposed by Niebieskikwiat and Salamon [7] was used to fit the H_{cool} dependence of M_E/M_S, where the satisfactory fit is shown in figure 7 by the broken curve. The number density of FM clusters is thus obtained from the fit as $n \approx 32.5 \times 10^{-5}$ Å^{-3}, which gives a rough estimate of the size of the FM clusters around ∼40 Å. The analysis indicates that the average size of the FM clusters is increased considerably for $x = 0.40$ than $x = 0.20$.

The temperature variation of resistivity (ρ) for the samples with $x = 0.20$ and 0.40 is shown in the upper and lower insets of figure 8, respectively. The semiconducting temperature dependence of ρ is observed for $x = 0.20$, while for $x = 0.40$ a nearly linear temperature dependence of ρ is observed in the paramagnetic state and a sharp decrease of ρ is observed

below T_C at 200 K. Temperature dependence of ρ for both samples is similar to the reported results [18], except for the magnitude of ρ. The slightly larger values of the resistivity in the present investigations might be attributed to the particle size effect, where the particle size in the present observation ($\sim$150 nm) is less than that for the results reported by Stauffer *et al* [18]. For $x = 0.20$ the system is close to the percolation limit, where the hole rich FM clusters are of small size but grow and coalesce with increasing x. Therefore, the average size of the FM clusters for $x = 0.40$ is larger than that of the sample with $x = 0.20$, which is reflected in the temperature dependence of resistivity and the analysis of the H_{cool} dependence of M_E/M_S. The size of the FM clusters is also crucial for the EB effect. The hysteresis loops measured at 5 K under identical conditions with $H_{cool} = 20$ kOe are shown in figure 8 for $x = 0.20$ and 0.40. The values of H_E and M_E/M_S are 82 Oe and 0.55×10^{-2} for $x = 0.40$, while for $x = 0.20$ the values are 500 Oe and 0.53×10^{-2}, respectively (see table 1). In addition, the magnetization at 50 kOe and H_C is 28.55 emu g^{-1} and 8.7 kOe for $x = 0.40$ and 23.92 emu g^{-1} and 13.0 kOe for $x = 0.20$, respectively. The values of magnetization at 50 kOe indicate that the size and density of the FM clusters are increased for $x = 0.40$ compared to $x = 0.20$, which is reflected in H_E, where H_E is much smaller for $x = 0.40$. Similar features of the EB effect were observed for the particle size dependence of the EB phenomenon in the CG compound $LaMn_{0.7}Fe_{0.3}O_3$, where FM clusters are embedded in the SG matrix [16]. The sizes of the FM clusters were found to increase with increasing particle size, which resulted in a decrease in the EB effect. A negligible EB effect was observed for the particles with average size $\sim$300 nm. The increase of the size of the FM clusters decreases the effective interface area, which might be the origin of the weakening of the effective exchange coupling at the FM/FI interface in the present investigations. This explanation is consistent with the model proposed by Meiklejohn, which predicts the relation $H_E \approx J_{ex}/(M_{FM}t_{FM})$, where J_{ex} is the exchange constant across the FM/AFM interface per unit area [37]. M_{FM} and t_{FM} are the magnetization and the thickness of the FM layer, respectively. The increase of M_{FM} and t_{FM} in the denominator of the above expression decreases the EB field. In the present investigation the average size of the FM clusters, analogous to t_{FM}, is increased for $x = 0.40$ compared to $x = 0.20$, which results in a decrease of the EB field.

4. Summary

As far as we are aware, we have observed for the first time the signature of the EB effect in $Nd_{1-x}Sr_xCoO_3$ for $x = 0.20$ and 0.40 at the spontaneous FM/FI interface. When the sample was cooled in a static magnetic field, the systematic shifts of the magnetic hysteresis loops are observed as a function of temperature and cooling field. The EB effect vanishes above the FI transition (T_{FI}) temperature, which indicates that the FI spins apply a pinning force on the reversible FM spins at the interface below T_{FI} and the pinned FM spins give rise to the EB phenomenon. The EB is further confirmed by the training effect, which could be explained satisfactorily by the spin configurational relaxation model. The EB field is found to increase sharply ($\leqslant$10 kOe) with increasing cooling field and then it shows a very small decreasing trend ($\geqslant$20 kOe) for high cooling fields. The coercivity almost follows a similar trend to the EB field, where a linear dependence of the EB field and coercivity against cooling field is observed above 20 kOe for both compounds. The dependence of the EB effect on the cooling field is analyzed by the simplified exchange interaction model, which gives a rough estimate of the average size of the FM clusters around $\sim$20 and $\sim$40 Å, where the FM clusters consisting of a single magnetic domain are suggested for $x = 0.20$ and 0.40, respectively. The sizes of the FM clusters are close to the percolation threshold for $x = 0.20$; they grow and coalesce with increasing x. The large size of the FM clusters leads to the weak EB effect for $x = 0.40$.

Acknowledgments

One of the authors (SG) wishes to thank DST (project no. SR/S2/CMP-46/2003), India for the financial support. The particle size of the samples were measured by TEM under the scheme of Nanoscience and Nanotechnology Initiative of DST at IACS, Kolkata, India. The authors wish to thank Mr A Karmakar for the English corrections. MP also wishes to thank CSIR for a SRF fellowship.

References

[1] Meiklejohn W H and Bean C P 1956 *Phys. Rev.* **102** 1413
[2] Stamps R L 2000 *J. Phys. D: Appl. Phys.* **33** R247
[3] Kiwi M 2001 *J. Magn. Magn. Mater.* **234** 584
[4] Nogues J, Sort J, Langlais V, Skumryev V, Surinach S, Munoz J S and Baro M D 2005 *Phys. Rep.* **422** 65
Nogues J, Sort J, Langlais V, Skumryev V, Surinach S, Munoz J S and Baro M D 2005 *Int. J. Nanotechnol.* **2** 23
Nogues J and Schuller I K 1999 *J. Magn. Magn. Mater.* **192** 203
[5] Berkowitz A E and Takano K 1999 *J. Magn. Magn. Mater.* **200** 552
[6] Kouvel J S 1961 *J. Phys. Chem. Solids* **21** 57
[7] Niebieskikwiat D and Salamon M B 2005 *Phys. Rev.* B **72** 174422
[8] Qian T, Li G, Zhang T, Zhou T F, Xiang X Q, Kang X W and Lia X G 2007 *Appl. Phys. Lett.* **90** 012503
[9] Patra M, De K, Majumdar S and Giri S 2007 *Eur. Phys. J.* B **58** 367
[10] Tang Y K, Sun Y and Cheng Z H 2006 *Phys. Rev.* B **73** 174419
[11] Tang Y K, Sun Y and Cheng Z H 2006 *J. Appl. Phys.* **100** 023914
[12] De K, Patra M, Majumdar S and Giri S 2008 *J. Phys. D: Appl. Phys.* **41** 175007
[13] De K, Ray R, Panda R N, Giri S, Nakamura H and Kohara T 2005 *J. Magn. Magn. Mater.* **288** 339
[14] De K, Patra M, Majumdar S and Giri S 2007 *J. Phys. D: Appl. Phys.* **40** 7614
[15] Liu X J, Li Z Q, Yu A, Liu M L, Li W R, Li B L, Wu P, Bai H L and Jiang E Y 2007 *J. Magn. Magn. Mater.* **313** 354
[16] Thakur M, Patra M, De K, Majumdar S and Giri S 2008 *J. Phys.: Condens. Matter* **20** 195215
[17] Patra M, Thakur M, De K, Majumdar S and Giri S 2008 *J. Phys.: Condens. Matter* **21** 078002
[18] Stauffer D D and Leighton C 2004 *Phys. Rev.* B **70** 214414
[19] Krimmel A, Reehuis M, Paraskevopoulos M, Hemberger J and Loidl A 2001 *Phys. Rev.* B **64** 224404

[20] Paraskevopoulos M, Hemberger J, Krimmel A and Loidl A 2001 *Phys. Rev.* B **63** 224416
[21] Yoshii K, Nakamura A, Abe H, Mizumaki M and Muro T 2002 *J. Magn. Magn. Mater.* **239** 85
Yoshii K and Abe H 2003 *Phys. Rev.* B **67** 094408
[22] Fondado A, Breijo M P, Rey-Cabezudo C, Sanchez-Andujar M, Mira J, Rivas J and Senaris-Rodriguez M A 2001 *J. Alloys Compounds* **323–324** 444
[23] Ghoshray A, Bandyopadhyay B, Ghoshray K, Morchshakov V, Barner K, Troyanchuk I O, Nakamura H, Kohara T, Liu G Y and Rao G H 2004 *Phys. Rev.* B **69** 064424
[24] Wu J and Leighton C 2003 *Phys. Rev.* B **67** 174408
[25] Geshev J 2008 *J. Magn. Magn. Mater.* **320** 600
[26] Salazar-Alvarez G, Sort J, Suriñach S, Baró M D and Nogués J 2007 *J. Am. Chem. Soc.* **129** 9102
[27] Del Bianco L, Fiorani D and Testa A M 2007 *J. Magn. Magn. Mater.* **310** 2289
[28] Hoffman A 2008 *Phys. Rev. Lett.* **93** 097203
[29] Binek C 2004 *Phys. Rev.* B **70** 014421
[30] Canet F, Mangin S, Bellouard C and Piecuch M 2000 *Europhys. Lett.* **52** 594
[31] Mangin S, Montaigne F and Schuhl A 2003 *Phys. Rev.* B **68** 140404(R)
[32] Berkowitz A E, Rodriguez G F, Hong J I, An K, Hyeon T, Agarwal N, Smith D J and Fullerton E E 2008 *Phys. Rev.* B **77** 024403
[33] Hauet T, Borchers J A, Mangin P, Henry Y and Mangin S 2006 *Phys. Rev. Lett.* **96** 067207
[34] Cai J W, Liu K and Chien C L 1999 *Phys. Rev.* B **60** 72
[35] Del Bianco L, Fiorani D, Testa A M, Bonetti E and Signorini L 2004 *Phys. Rev.* B **70** 052401
Fiorani D, Bianco Del L, Testa A M and Trohidou K N 2007 *J. Phys.: Condens. Matter* **19** 225007
[36] Markovich V, Fita I, Wisniewski A, Puzniak R, Mogilyansky D, Titelman L, Vradman L, Herskowitz M and Gorodetsky G 2008 *Phys. Rev.* B **77** 054410
[37] Meiklejohn W H 1962 *J. Appl. Phys.* **33** 1328